Disulphide-reduced psoriasin is a human apoptosis-inducing broad-spectrum fungicide

Kyaw Zaw Hein[a,1], Hitoshi Takahashi[a], Toshiko Tsumori[b,c], Yukihiko Yasui[c], Yasuko Nanjoh[d], Tetsuo Toga[d], Zhihong Wu[e], Joachim Grötzinger[f], Sascha Jung[f], Jan Wehkamp[g,h,2], Bjoern O. Schroeder[g,3], Jens M. Schroeder[e,4,5], and Eishin Morita[a,4,5]

[a]Department of Dermatology, Faculty of Medicine, Shimane University, Izumo 693-8501, Japan; [b]Department of Nursing, Faculty of Health and Welfare, Prefectural University of Hiroshima, Mihara 723-0053, Japan; [c]Department of Anatomy and Morphological Neuroscience, Faculty of Medicine, Shimane University, Izumo 693-8501, Japan; [d]Research Center, Nihon Nohyaku Co., Ltd., Kawachi-Nagano, Osaka 586-0094, Japan; [e]Department of Dermatology, University-Hospital Schleswig-Holstein, 24105 Kiel, Germany; [f]Institute of Biochemistry, Christian-Albrechts-University, 24098 Kiel, Germany; [g]Dr. Margarete Fischer-Bosch-Institute of Clinical Pharmacology, University of Tübingen, 70376 Stuttgart, Germany; and [h]Department of Internal Medicine 1, Robert-Bosch Hospital, 70376 Stuttgart, Germany

Edited by David M. Underhill, Cedars Sinai Medical Center, Los Angeles, CA, and accepted by the Editorial Board August 28, 2015 (received for review June 11, 2015)

The unexpected resistance of psoriasis lesions to fungal infections suggests local production of an antifungal factor. We purified *Trichophyton rubrum*-inhibiting activity from lesional psoriasis scale extracts and identified the Cys-reduced form of S100A7/psoriasin (redS100A7) as a principal antifungal factor. redS100A7 inhibits various filamentous fungi, including the mold *Aspergillus fumigatus*, but not *Candida albicans*. Antifungal activity was inhibited by Zn^{2+}, suggesting that redS100A7 interferes with fungal zinc homeostasis. Because S100A7-mutants lacking a single cysteine are no longer antifungals, we hypothesized that redS100A7 is acting as a Zn^{2+}-chelator. Immunogold electron microscopy studies revealed that it penetrates fungal cells, implicating possible intracellular actions. In support with our hypothesis, the cell-penetrating Zn^{2+}-chelator TPEN was found to function as a broad-spectrum antifungal. Ultrastructural analyses of redS100A7-treated *T. rubrum* revealed marked signs of apoptosis, suggesting that its mode of action is induction of programmed cell death. TUNEL, SYTOX-green analyses, and caspase-inhibition studies supported this for both *T. rubrum* and *A. fumigatus*. Whereas redS100A7 can be generated from oxidized S100A7 by action of thioredoxin or glutathione, elevated redS100A7 levels in fungal skin infection indicate induction of both S100A7 and its reducing agent in vivo. To investigate whether redS100A7 and TPEN are antifungals in vivo, we used a guinea pig tinea pedes model for fungal skin infections and a lethal mouse *Aspergillus* infection model for lung infection and found antifungal activity in both in vivo animal systems. Thus, selective fungal cell-penetrating Zn^{2+}-chelators could be useful as an urgently needed novel antifungal therapeutic, which induces programmed cell death in numerous fungi.

antifungal | innate immunity | epithelial defense | psoriasin | S100A7

Fungi cause emerging infectious diseases that increasingly threaten human health (1–3). Superficial fungal infections affect 20–25% of the global population and opportunistic fungal infections cause serious medical problems, with high morbidity and mortality, particularly in immunocompromised patients (3, 4). Filamentous fungi are composed of a conidium, an asexual spore, and a hypha, a long, branching filamentous structure. Conidia, which are ubiquitously spread in soil and air, represent the primary infectious unit of fungi. Therefore, it is amazing that the permanent exposure and colonization of our body surfaces by various fungi (5) does not usually cause infections in healthy individuals. Surprisingly, it is largely unknown how and why human body surfaces resist fungal pathogens.

Healthy human lungs are highly efficient at clearing airborne fungal spores without causing lung inflammation, suggesting that innate defense strategies to control fungal pathogens do exist in the epithelium (6). Epithelial antimicrobial peptides are the candidate effector molecules that could play a role in defending the body against fungal infections. Although the disulphide-reduced form of human β-defensin-1 (hBD-1) shows—apart from its bactericidal activity—strong activity against *Candida albicans* (7), there is no systematic study investigating antifungals with human epithelial origin that might control the growth of filamentous fungi at body surfaces.

To address this important question, we analyzed lesional skin from patients with psoriasis—a skin disease with an unexpected resistance to fungal infections (8)—in an attempt to identify human antifungals (9, 10).

Results

Identification of Disulphide-Reduced Psoriasin as Antifungal Protein. Human epithelia show a marked resistance toward bacterial and fungal infections, particularly skin lesions of psoriasis patients,

Significance

Fungi increasingly cause serious medical problems in immunocompromised populations. Antimicrobial peptides are primary effector molecules of innate immune systems. Antimicrobial peptides successfully protect healthy humans from bacterial infections. However, it is largely unknown how and why human body surfaces resist fungal infections. We identified the common epithelial protein, psoriasin (S100A7), in its disulphide-reduced form (redS100A7) as the principal antifungal factor of human body surfaces. redS100A7 kills several pathogenic fungi using a mechanism that differs from conventional antifungal agents. Thus, this study might contribute to a better understanding of human defense systems against fungal infection and the development of urgently needed novel antifungal therapeutics.

Author contributions: K.Z.H., J.M.S., and E.M. designed research; K.Z.H., H.T., T. Tsumori, Y.Y., Y.N., T. Toga, Z.W., J.G., S.J., and B.O.S. performed research; Z.W. contributed new reagents/analytic tools; K.Z.H., T. Tsumori, Y.Y., Y.N., T. Toga, J.G., S.J., J.W., B.O.S., J.M.S., and E.M. analyzed data; and K.Z.H., J.M.S., and E.M. wrote the paper.

Conflict of interest statement: K.Z.H., E.M., and J.M.S. filed a patent on reduced psoriasin as fungicide.

This article is a PNAS Direct Submission. D.M.U. is a guest editor invited by the Editorial Board.

[1]Present address: Robert and Arlene Kogod Center on Aging, Mayo Clinic, Rochester, MN 55905.

[2]Present address: Department of Internal Medicine I, University of Tuebingen, 72076 Tuebingen, Germany.

[3]Present address: Wallenberg Laboratory, University of Gothenburg, 413 45 Gothenburg, Sweden.

[4]J.M.S. and E.M. contributed equally to this work.

[5]To whom correspondence may be addressed. Email: jschroeder@dermatology.uni-kiel.de or emorita@med.shimane-u.ac.jp.

This article contains supporting information online at www.pnas.org/lookup/suppl/doi:10.1073/pnas.1511197112/-/DCSupplemental.

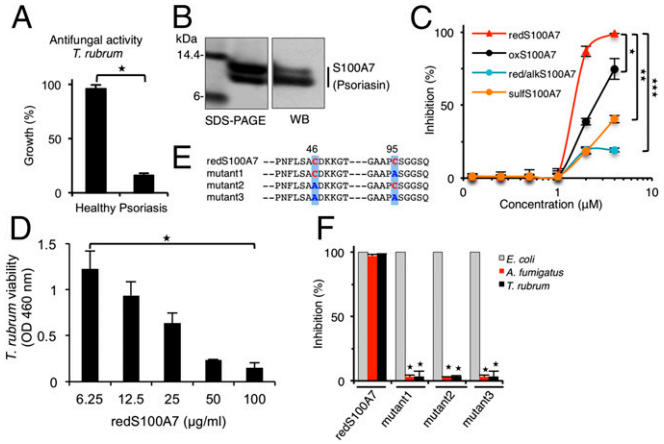

Fig. 1. Identification of reduced S100A7 (redS100A7) as an antifungal protein. (*A*) Psoriatic scale extracts contain *T. rubrum* antifungal activity ($n = 3$ $*P < 0.001$). (*B*) SDS/PAGE and Western blot (WB)-analyses of the antifungal protein purified from the psoriasis scales. (*C*) redS100A7 is a potent antifungal protein compared with oxS100A7, reduced and alkylated S100A7 (red/alkS100A7), and S-sulfito-S100A7 (sulfS100A7). $*P < 0.01$, $**P < 0.007$ and $***P < 0.001$. (*D*) redS100A7 decreases cell viability in *T. rubrum* dose-dependently. Viable fungi were detected by the MTT tetrazolium salt colorimetric assay. $n = 3$ independent experiments. Mean ± SD is shown. $*P < 0.008$. (*E*) Partial ascorbic acid (AA) sequences of redS100A7 and the three mutants. (*F*) Whereas antifungal activity is absent in all three Cys-Ala-mutants ($*P < 0.002$), antibacterial activity is still present. A minimum of three independent experiments was performed and the average ± SD is plotted.

which are unexpectedly rarely affected (8, 10). We hypothesized that antifungal activity is generated in psoriasis lesions. We analyzed psoriatic scale extracts and found *Trichophyton rubrum* growth inhibiting activity (Fig. 1*A*). The antifungal agent was purified by several HPLC steps to homogeneity (Fig. S1).

SDS/PAGE, Western blot analyses (Fig. 1*B*), protein-sequencing, and MALDI-MS analyses revealed that the antifungal protein was the reduced form of psoriasin, S100A7. Inhibition of antifungal activity by psoriasin antibodies (Fig. S1*G*) excluded a copurifying contaminant.

Two Free Cysteines of S100A7 Are Essential for Antifungal Activity. Different bands upon SDS/PAGE analyses revealed easy air oxidation of *S100A7* (Fig. 1*B*). Reduction of the single disulphide bridge in oxS100A7 results in two free-thiol groups of the cysteine residues, Cys46 and Cys95. To elucidate the involvement of these thiol groups in the antifungal effect, we analyzed the reduced and alkylated S100A7 (red/alkS100A7) and found very low antifungal activity (Fig. 1*C*), suggesting that free thiols are essential. Viability tests after redS100A7-treatment of *T. rubrum* indicated that it acts as a fungicidal agent (Fig. 1*D*). We then generated S100A7 mutants, in which either one or both cysteines were substituted with alanine (Fig. 1*E*). All three mutants, the Cys95Ala-S100A7 (mutant 1), Cys46Ala-S100A7 (mutant 2), and Cys46Ala, Cys95Ala-S100A7 (mutant 3) did not show any inhibition of *T. rubrum* growth (Fig. 1*F*). Interestingly, the growth of *Escherichia coli* was similarly inhibited, as seen with oxS100A7 (11) (Fig. 1*F*), corroborating that both free thiols are essential for antimycotic but not bactericidal activity.

redS100A7 Chelates Zn^{2+} Ions in Fungi. oxS100A7 is highly abundant on healthy human skin and several mucosal surfaces (11–13). Its antibacterial activity is Zn^{2+}-sensitive, acting via a histidine-coordinated low-affinity Zn^{2+}-binding site (14). Correspondingly, we found that Zn^{2+} completely inhibited the antifungal activity of redS100A7 (Fig. 2*A*), whereas other divalent ions did not reduce antifungal activity.

With few exceptions, protein zinc-binding sites are Cys, His, or Glu/Asp (15). To elucidate whether opening the disulphide bond of oxS100A7 causes secondary structure changes, we performed circular dichroism (CD) spectroscopy. Without exposure to Zn^{2+}, redS100A7 displayed a CD spectrum of α-helical structural elements, which is similar to that of oxS100A7 (16) (Fig. 2*B*). However, Zn^{2+}-exposure causes a shift of the CD spectrum (Fig. 2*B*), supporting the hypothesis that Zn^{2+} produces a conformation change. Because the low-affinity Zn^{2+}-binding site of oxS100A7 is formed via four His of an oxS100A7 dimer (14), we analyzed Zn^{2+}-treated redS100A7 through electrospray ionization-mass spectrometry (ESI-MS) and found a mass of 22,958 Da, corresponding to a redS100A7 dimer plus Zn^{2+}ions (Fig. S1*H*). This finding supports the hypothesis that four thiols in two redS100A7 molecules bind Zn^{2+}, suggesting formation of a new Zn^{2+}-binding site in redS100A7. This hypothesis was corroborated by the finding that Ca^{2+} augmented the antifungal efficacy of redS100A7 (Fig. S2*A*), because Ca^{2+} increases the Zn^{2+}-binding affinity of the S100A8/A9 complex calprotectin (17).

To examine whether redS100A7 chelates Zn^{2+} in fungi, we incubated redS100A7-treated *T. rubrum* with Zinquin, a cell-permeable fluorescent probe specific for Zn^{2+} ions (18, 19), and observed an alteration in Zinquin staining pattern (Fig. 2*C*). This finding suggests that redS100A7 results in altered subcellular distribution of labile zinc. Together with the data presented in Fig. 2 *A* and *B*, this suggests that redS100A7 acts as a natural Zn^{2+}-chelator. To test this hypothesis, we investigated synthetic Zn^{2+}-chelators, and identified the cell-membrane–permeable Zn^{2+}-chelator TPEN [N,N,N′,N′-Tetrakis(2-pyridylmethyl)- ethylenediamine] (20) as a potent antifungal (Fig. 2*D*).

redS1007 and TPEN Are Broad-Spectrum Fungicides. Next we analyzed the effects of redS100A7 on other fungi. redS100A7 inhibited the growth of several filamentous fungi and yeasts, such as *Aspergillus fumigatus*, *Malassezia furfur*, *Microsporum canis*, *Rhizopus oryzae*, *Saccharomyces cerevisiae*, and *Trichophyton mentagrophytes* with a 90% minimal inhibitory concentration (MIC_{90}) of ~2 μM (Fig. 3*A*). However, the yeast *C. albicans* was not affected at concentrations up to 20 μM, which is surprising

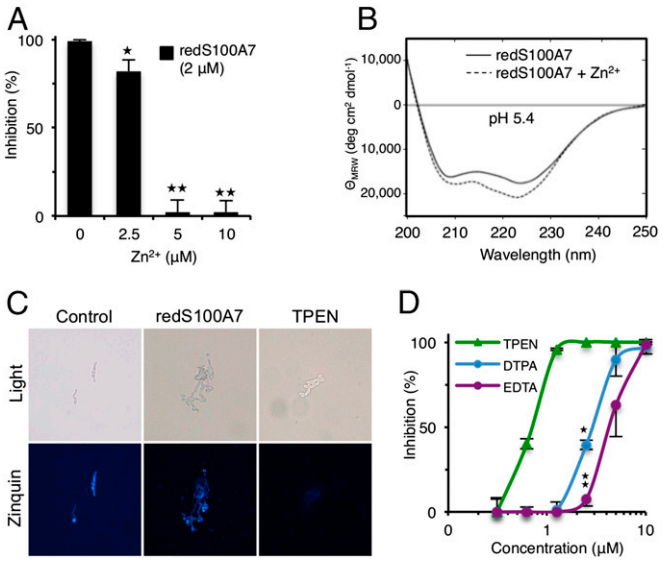

Fig. 2. redS100A7 sequesters Zn^{2+} ions in fungal cells. (*A*) redS100A7 antifungal activity is inhibited by addition of Zn^{2+} ($*P < 0.05$, $**P < 0.001$ vs. 0 μM Zn^{2+}). (*B*) CD spectroscopy of redS100A7 at pH 5.4 in the presence or absence of Zn^{2+}. Note changes in α-helical content characterized by a deep minimum between 209 and 222 nm. (*C*) In redS100A7-treated *T. rubrum*, intracellular liable Zn^{2+} are stained with a specific fluorescent probe, Zinquin. (Magnification: 300×.) (*D*) Antifungal activity (*T. rubrum*) of different Zn^{2+}-chelators. TPEN is a cell-permeable chelator, and DTPA and EDTA are cell-impermeable chelators ($*P < 0.002$, $**P < 0.001$). A minimum of three independent experiments was performed and the average ± SD is plotted.

because *C. albicans* is killed by calprotectin in a Zn^{2+}-dependent fashion (21). We identified TPEN (20) as a broad-spectrum antifungal agent that kills a high variety of filamentous fungi and yeasts, including *C. albicans*, at a MIC_{90} of ~2 μM for all tested fungi (Fig. 3*B*), which supports our hypothesis that redS100A7 acts as a natural fungus cell-penetrating Zn^{2+}-chelator.

redS100A7 and TPEN Kill Fungi by Inducing Apoptosis-Like Cell Death. To analyze the mechanism underlying redS100A7 antimycotic activity, redS100A7-treated *T. rubrum* conidia were analyzed for intracellular reactive oxygen species (ROS) levels. Levels increased in a dose-dependent manner (Fig. 3*C*) and inhibition of the activity by a ROS-inhibitor ascorbic acid (Fig. S2*C*) suggest that antifungal activity is at least in part ROS-mediated. We excluded the fungal copper/zinc superoxide dismutase (Cu/Zn-SOD) (22), the SOD enzyme (Fig. S2*D*), and the fungal sterol biosynthesis (Fig. S2*E*), as primary targets of redS100A7 antifungal action.

To investigate whether redS100A7 causes apoptosis in fungal cells, DNA degradation was visualized using a TUNEL assay. After 4 h of exposure, redS100A7-treated *T. rubrum* and *A. fumigatus* showed $TUNEL^+$ phenotypes representing apoptotic DNA breaks (Fig. 3*D*, *Left*). In *T. rubrum* cells, 24-h exposure to redS100A7 affected the plasma membrane integrity, as evidenced by a strong, intact plasma membrane-impermeable SYTOX-green nucleic acid staining in mycelia (Fig. 3*D*, *Right*). Similar findings were obtained when *T. rubrum* and *A. fumigatus* were treated with TPEN (Fig. 3 *D* and *E*).

redS100A7- and TPEN-Treated Fungi Show Signs of Apoptosis-Like Cell Death. Further support of apoptosis induction in fungal cells by both redS100A7 and TPEN came from ultrastructural analyses by transmission electron microscopy (TEM). We found dark nuclei with dilated nucleolemmal cisterns, degraded mitochondria, electron-dense depositions, lipid droplets, and blebs in the plasma membrane in *T. rubrum* treated with redS100A7 for 24 h (Figs. 3*F* and 4*C*).

We then investigated the ultrastructure of redS100A7- and TPEN-treated *A. fumigatus* by scanning electron microscopy (SEM). redS100A7 and TPEN treatments cause shrunken filaments and damaged fungal spores (conidia), premature conidia, and open-ended amphora-like conidia-producing phialides (Fig. 3 *G* and *H* and Fig. S3).

To confirm whether redS100A7 induces apoptotic cell death in fungi, we coincubated redS100A7 with a cell-permeant pan caspase inhibitor (Z-VAD-FMK) (23) and found dose-dependent inhibition of the redS100A7-induced cell death in *T. rubrum*, suggesting that redS100A7 kills fungi via a caspase-dependent apoptosis pathway (Fig. 3*I*).

Next, we determined the target location of redS100A7-treated *T. rubrum* and *A. fumigatus*. These fungi were incubated with S100A7 antibodies and then analyzed using immunofluorescence (IF) confocal microscopy and immunogold TEM. IF-S100A7 was seen to accumulate at the surface of and within conidia of *T. rubrum* (Fig. 4*A*), as well as in the conidia and along the hyphae of *A. fumigatus* (Fig. 4*B*). Ultrastructural analyses by immunogold TEM revealed redS100A7 along the outer surface of the cell wall, as well as penetrating the fungal cell near a conidium or within conidia (Fig. 4*C* and Fig. S4). Thus, it suggests that redS100A7 first accumulates at the conidium surface and then penetrates fungal membranes close to the conidium, corroborating that conidia are the primary target of redS100A7.

redS100A7 Is Generated During Dermatophyte Skin Infection. To investigate whether redS100A7 acts in vivo, we investigated S100A7 levels in the stratum corneum of healthy and dermatophyte-infected skin. The amounts of S100A7 increased threefold in the dermatophyte-infected patients (Fig. S5*A*). To determine the redox status of S100A7, stratum corneum extracts from both groups were immediately alkylated and then analyzed by MALDI-MS. Markedly increased amounts of redS100A7, compared with healthy controls, were seen in lesional dermatophyte-infected skin (Fig. S5*B*), indicating an induction and local reduction of oxS100A7 to redS100A7 in response to fungal infections.

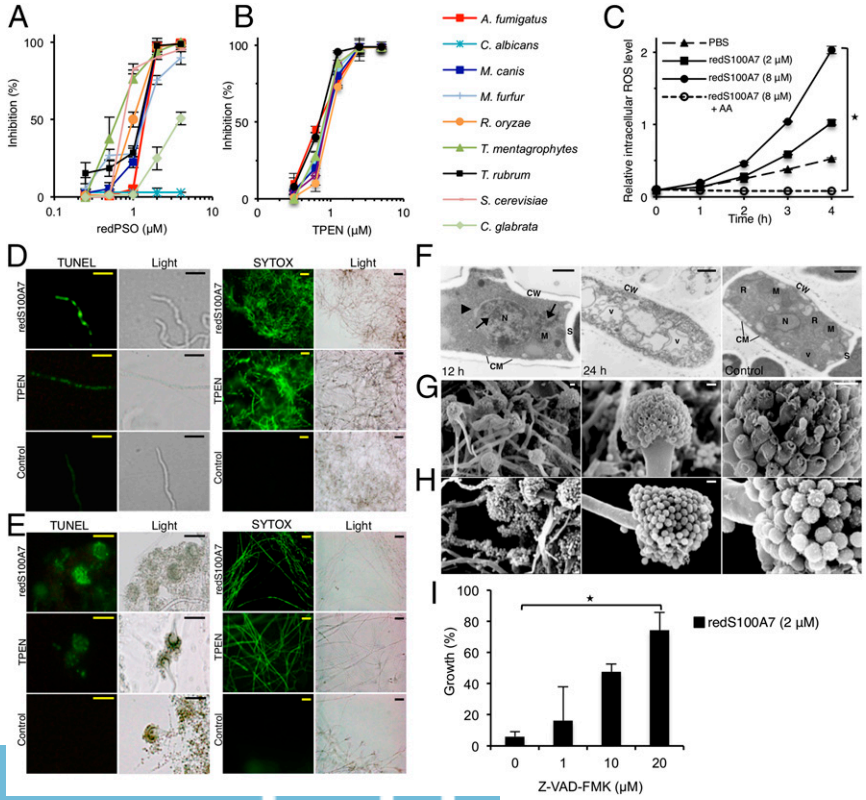

Fig. 3. Action mechanism of redS100A7. (*A*) Broad-spectrum antifungal activity of redS100A7 against various fungi. (*B*) Broad-spectrum antifungal activity of TPEN. (*C*) Intracellular ROS (determined with the fluorescent probe carboxy-H2DCFA) were dose-dependently raised in redA100A7-treated conidia. The ROS-inhibitor AA prevented the ROS-generation (4 h, $*P < 0.0003$, $n = 3$ independent experiments). (*D*) TUNEL assay (to observe DNA fragmentation) and SYTOX-green staining (to observe disintegrated plasma membrane) of redS100A7-treated (4 μM) *T. rubrum*. (Scale bars, 20 μm.) (*E*) TUNEL assay and SYTOX-green staining of redS100A7-treated (4 μM) *A. fumigatus*. (Scale bars, 20 μm.) (*F*) TEM images of redS100A7 (4 μM)-treated *T. rubrum*. Arrows indicate electron-dense depositions and arrowhead represents dilated nucleolemmal cisterns. (Scale bars, 0.2 μm.) (*G* and *H*) SEM analyses of redS100A7-treated (4 μM) *A. fumigatus* (*G*) and controls (*H*). Note destroyed fungal spores (conidia), premature conidia and conidia-producing phialides (circle). (Scale bars, 2 μm.) CM, cell membrane; CW, cell wall; M, mitochondria; N, nucleus; R, ribosomes; V, vacuole. (*I*) A cell-permeant pan caspase inhibitor blocks the antifungal activity of redS100A7 in a dose-dependent manner. ($n = 3$ independent experiments, $*P < 0.02$.)

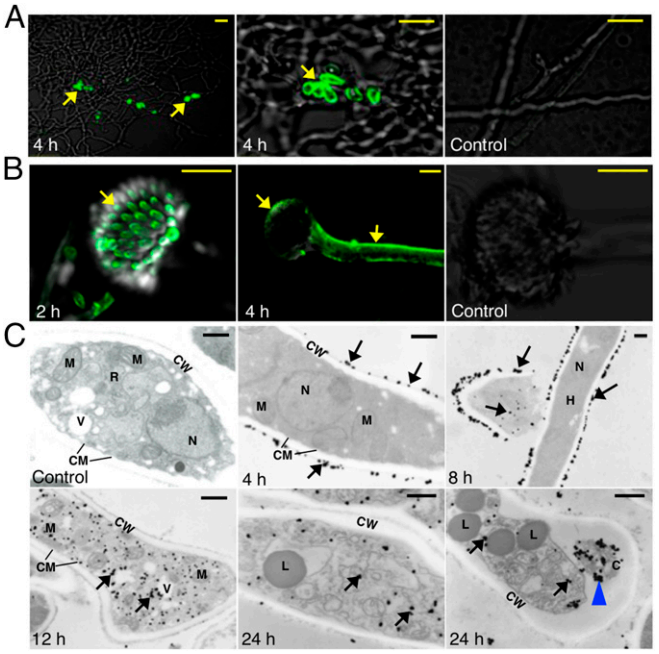

Fig. 4. Target localization of redS100A7. (*A*) redS100A7-immunofluorescence visualization (arrows) on *T. rubrum* by confocal laser microscopy. Note redS100A7 accumulation on conidia (arrows). (Scale bars, 50 μm.) (*B*) Confocal laser microscopy of 2 h (*Left*) or 4 h (*Center*)-treated *A. fumigatus*. Arrows indicate the location of redS100A7 on conidia at 2 h and hyphae at 4 h. (Scale bars, 50 μm.) (*C*) Immunogold labeling electron microscopy (*Upper* and *Lower*). Arrows point toward gold particles that represent redS100A7 immune complexes. Arrowhead indicates gold particles accumulating within the conidia. (Scale bars, 0.2 μm.) C, conidium; CM, cell membrane; CW, cell wall; H, Hyphae; L, lipid droplet; M, mitochondria; N, nucleus; R, ribosomes; V, vacuole. Independent experiments have been repeated at least three times and showed similar results.

Thioredoxin and Reduced Glutathione Generate redS100A7. Next we analyzed the mechanism of redS100A7 generation. Epidermis has a very high antioxidant capacity because of high levels of reduced glutathione (GSH) (24) and thioredoxin (TRX) (7, 24). In gut mucosa and skin, the TRX-reductase (R) system regulates physiologically relevant oxidoreduction (25, 26). We found that the TRX-R system dose-dependently increased the amount of redS100A7 (Fig. S5*C*). Interestingly, GSH alone also generated redS100A7 (Fig. S6).

Sulfitation-Dependent Inactivation of Psoriasin Is Reversed by the TRX System. Dermatophytes are specialized fungi that live in the stratum corneum, where they subsist on cysteine-rich proteins like keratins. These fungi secrete sulfite to make stratum corneum proteins digestible, forming S-sulfito-cysteines before proteolysis (27). As expected, we found the disulphide-bridge of oxS100A7 to be cleaved, forming the single thiol-group–containing S-sulfito-S100A7 during *T. rubrum* culture in vitro (Fig. S7). The S-sulfito-S100A7 showed low antifungal activity (Fig. 1*C*), which supports our finding that a single thiol-containing S100A7 mutant is inactive (Fig. 1*F*). These experiments indicate that *T. rubrum* and other sulfite-generating fungi can inactivate S100A7. However, S-sulfito-S100A7 was not detected in the lesional stratum corneum obtained from dermatophyte skin infections (Fig. S5), which suggests that in vivo the host-derived redox system converts it to redS100A7. To address this, we incubated S-sulfito-S100A7 with TRX-R and found its complete reduction toward redS100A7 (Fig. S7).

Surprisingly oxS100A7 is also an antifungal that requires higher concentrations than redS100A7, however (Fig. 1*C*). One would have expected that complete absence of antifungal activity might be because of the lack of two free-thiol groups in oxS100A7. Therefore, intracellular oxS100A7 within the fungal cells and the endogenously produced intermediate S-sulfito-S100A7 should be reduced in situ toward redS100A7. IF-analyses with the inactive Cys46Ala-S100A7 mutant (which is recognized by the S100A7 antibody) indicate that oxS100A7 should also penetrate fungal cell membranes (Fig. S4*F*), which suggests that it is reduced within the cell. To test this theory, we added increasing amounts of oxidized GSH (GSSG), a competing disulphide-bond–containing compound, and found a dose-dependent decrease of oxS100A7 antifungal activity (Fig. S7).

redS100A7 and TPEN Are Protective in a *T. mentagrophytes* Guinea Pig Tinea Pedes Model. To investigate whether redS100A7 and TPEN also act in vivo, we generated a guinea pig model of tinea pedis (28). An ablated guinea pig foot was treated with redS100A7, TPEN, or the vehicle. The foot was then infected with 1.5×10^7 *T. mentagrophytes* conidia. After 3 d of infection, the infected areas were analyzed microscopically, and with Periodic acid Schiff (PAS) reagent and Fungiflora Y staining. Fungal invasion into the stratum corneum was recorded. Both redS100A7 and TPEN showed a significant protective effect in the guinea model of *T. mentagrophytes* infection (Fig. 5 *A* and *B* and Fig. S8).

redS100A7 and TPEN Prevent Death in a Lethal *Aspergillus* Infection Mouse Model. Finally, we investigated the in vivo antifungal activity of redS100A7 in a mouse model of *Aspergillus* lung infection (29), in which immunocompromised mice were infected with 2×10^7 *A. fumigatus* conidia for 2 consecutive days. Whereas all mice in the control group did not survive the infection, mice in the redS100A7- or TPEN-treatment survived the invasive fungal infection throughout the 7-d observation period (Fig. 5*C*). Numerous *A. fumigatus* conidia and hyphae, as well as massive neutrophil infiltrates, were observed in the untreated control lungs after 3 d (Fig. 5*D* and Fig. S9). In contrast, fungal burdens were hardly found in redS00A7- or TPEN-treated mice (Fig. 5*D* and Fig. S9). However, lung histology showed massive inflammatory infiltrates, possibly as a result of dead and degenerating hyphae (Fig. 5*D* and Fig. S9).

Discussion

Lesional psoriatic skin contains the Cys-reduced form of psoriasin (S100A7) as a principal antifungal component, which has antifungal activity against various pathogenic fungi. Although the Cys-oxidized form also shows antifungal activity, it is markedly less potent (Fig. 1), a fact that would explain our failure to purify the oxygen-sensitive Cys-reduced form of psoriasin. The finding that Cys-thiol–lacking S100A7 derivatives show less antifungal activity and S100A7 mutants lacking Cys are not fungicidal suggests that free-thiol groups are essential for the antifungal activity of S100A7 and points toward a unique mode of action of redS100A7. Antibacterial activity of oxS100A7 is mainly restricted toward *E. coli*; far lower activity was seen against *Pseudomonas aeruginosa* and *Staphylococcus aureus* (11), and in the oxS100A7 it is inhibited by Zn^{2+} at pH 7.4 (11). This finding suggests that the His-based Zn^{2+}-binding sites in the oxS100A7 (14) and in the Cys-Ala- S100A7 mutants are involved in *E. coli*-cidal activity at pH 7.4. However, at pH 5.5, the normal skin pH, where His-based Zn^{2+}-binding sites are inactive, oxS100A7 is bactericidal with a different mode of action, targeting the bacterial membrane by forming pores (16). redS100A7 is a potent antifungal at pH 5.5, but sensitive toward an alkaline pH (Fig. S1*I*). A plausible explanation for the antifungal activity of redS100A7 at an acidic pH, low stability at alkaline pH and Zn^{2+}-sensitivity would be the involvement of a Cys-thiol–based Zn^{2+}-binding site. This, however, would need the opening of the single disulphide group in S100A7, causing structural changes upon Zn^{2+}-binding (Fig. 2*B*). Our finding that both Cys-thiols in S100A7 are necessary for activity (Fig. 1) and redS100A7 forms Zn^{2+}-binding dimers at acidic pHs (Fig. S1) supports the idea that the Zn^{2+}-binding site could be of the $(Cys)_4$-type (15). Indeed, a previous study revealed inhibition of fungal growth by synthetic zinc chelators and calprotectin

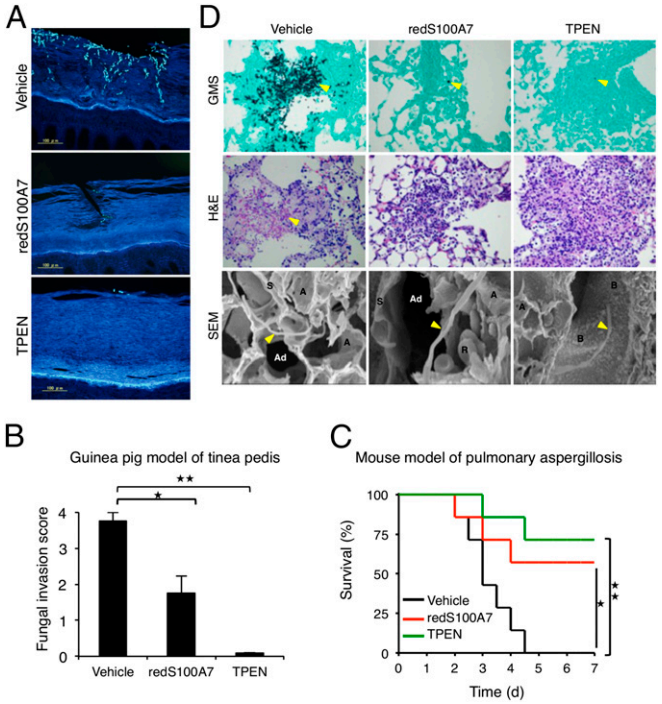

Fig. 5. In vivo antifungal activity of redS100A7 and TPEN. (*A* and *B*) After applied with vehicle, redS100A7 or TPEN, the plantar of guinea pigs was infected with *T. mentagrophytes*. Fungal invasion was determined histologically (*A*) and by scoring (*B*) (see *SI Materials and Methods*). ($n = 4$, $*P < 0.005$, $**P < 0.0001$). (*C*) Immunocompromised mice were infected with *A. fumigatus* and treated with redS100A7, TPEN, or the vehicle. The Kaplan–Meier survival curve comparing untreated control mice (black) with redS100A7-treated (red) and TPEN-treated mice (green) ($n = 7$ for each group, $*P < 0.036$ and $**P < 0.003$ vs. controls; log-rank test) is shown. (*D*) Histopathology and SEM analyses of mouse lungs infected with *A. fumigatus*. Arrowheads indicate *A. fumigatus*. Grocott's Methenamine Silver (GMS), H&E. A, alveolus; Ad, alveolar duct; B, bronchiole; R, red blood cell; S, septum. (Magnification: *D*, GMS and H&E, 200×; SEM, 1,700×.)

(S100A8/A9) (30). Therefore, a synthetic zinc-chelator should have antifungal activity. We tested three zinc chelators and identified the cell-penetrating zinc-chelator TPEN as the most potent antifungal with an ED_{50} at ~1 μM, similar as that seen for redS100A7 (Figs. 2 and 3). Because noncell-penetrating zinc chelators are the least-potent antifungals, this would indicate that intracellular zinc-chelation could be the mechanism behind redS100A7-dependent antifungal activity. To test this hypothesis, we investigated redS100A7-treated fungi with the fluorescent zinc sensor Zinquin, which allows monitoring of loosely bound, labile intracellular Zn^{2+} and which does not mobilize tightly bound Zn^{2+} from enzymes (18). We saw a stronger vesicle-associated fluorescence (Fig. 2*C*), a phenomenon also seen in apoptotic lymphocytes (19), but barely—if any—increase in fluorescence. Perhaps this unexpected finding is caused by the presence of two zinc binding sites with different affinities in redS100A7. In such a case Zinquin fluorescence analyses reveal complicated results, possibly because of the analyses' inability to report on two K_d values that differ by several orders-of-magnitude (31). One may speculate that redS100A7 enters the fungal cell, sequesters zinc from cytosolic sources, and then migrates to the endosomal compartments where zinc is released from redS100A7 (because of the local endosomal environment), resulting in increased labile zinc, which increases Zinquin fluorescence. The absence of similar fluorescence signals in TPEN-treated fungi is a result of TPEN's higher affinity toward Zn^{2+}, which causes quenching of the Zinquin-fluorescence (18).

We then investigated the mechanism underlying how redS100A7 kills fungi. redS100A7 has been shown to have fungicidal activity (Fig. 1*D*). Polyene antifungals (e.g., amphotericin B) and azole antifungals (e.g., fluconazole) are commonly used antifungal agents. Polyene antifungals bind to ergosterol in the fungal cell membrane, forming transmembrane channels that lead to monovalent ion leakage (32). Azole antifungals inhibit the fungal cytochrome P450 enzyme, preventing the formation of essential ergosterol (32). We observed that redS100A7 neither interacted with ergosterol nor inactivated fungal Cu/Zn-superoxide dismutases for its antifungal action (Fig. S2). Instead, ultrastructural analyses (Fig. 3*F*) of redS100A7-treated fungi suggest that it induces apoptosis-like cell death in fungi. Indeed, TUNEL analyses, SYTOX-green analyses, and inhibition of fungicidal activity by a caspase inhibitor (Fig. 3*I*), as well as the Zinquin-experiments (Fig. 2) corroborated the hypothesis that it induces apoptosis-like cell death in fungi in a zinc-dependent manner. Zinc plays an important role in the regulation of apoptosis. It has been shown that the addition of Zn^{2+}-chelators leads to apoptosis-induction in various hepatocytes, as well as in leukemia cells (33, 34). Sequestering inhibitory Zn^{2+} ions in inactive procaspase-3 generates active caspase-3, which subsequently triggers the downstream effector caspase-6 and induces apoptosis (33). We also demonstrated that redS100A7-induced fungal cell death is reversible through a pan caspase inhibitor (Fig. 3*I*). Therefore, in contrast to conventional antifungal agents, our data suggest that redS100A7 induces apoptosis-like fungal cell death, possibly via activation of the metacaspase system (i.e., the caspase system of fungi, plants, and protozoa) by sequestering zinc ions. However, further analyses are needed to prove this hypothesis.

Ultrastructural analyses (Fig. 3 *F–H*) suggest that the main target of redS100A7 could be conidia, the asexual nonmotile spores of a fungus. This finding was supported by both immunofluorescence-staining and immunogold detection of S100A7, accumulating at or close to conidia in *T. rubrum* and *A. fumigatus* (Fig. 4). Kinetic analyses revealed that redS100A7 is penetrating the fungal cell close to a conidium, then diffusing within the cell and eventually accumulating within the conidium (Fig. 4). It is tempting to speculate that the highly hydrophobic S100A7 accumulates at conidia of filamentous fungi because of the presence of hydrophobins (35, 36). The absence of hydrophobins in *C. albicans* (36) would explain the failure of redS100A7 to kill this yeast. We investigated the sensitivity of a hydrophobin mutant of *A. fumigatus* (37) but found no difference in sensitivity (Fig. S10), which suggests that either hydrophobin is not the target of S100A7 or other hydrophobins are still present.

If redS100A7 is an important antifungal defense component of human skin, one would expect it to form during fungal infection. Indeed, stratum corneum of patients with tinea pedes, a dermatophyte skin infection of the feet, revealed increased amounts during infection (Fig. S5). This finding was unexpected because dermatophytes are cleaving disulphide-bridges with sulfite, forming sulfitocysteines (27), as shown in oxS100A7 (Fig. S7). Skin has a negative redox potential (24), containing high amounts of reduced GSH (24) and TRX (7, 25). Because both redox-compounds are able to convert oxS100A7 and sulfito-S100A7 into antifungal redS100A7 (Figs. S5–S7), skin has an efficient counterstrategy to compensate dermatophyte's inactivation of S100A7. Thus, the presence of the TRX-R system, reduced hBD-1 (7), and GSH (24) in healthy skin suggests that S100A7 is also present in its reduced state.

S100A7 Cys-Ala mutants and other derivatives indicate that free Cys thiols are essential for antifungal activity (Fig. 1). Therefore, it is surprising that oxS100A7, which lacks free-thiol groups, is an antifungal. A possible explanation would be its disulphide-bridge reduction within the fungal cell by a fungal oxidoreductase. Although direct proof has yet to be collected, this hypothesis is supported by a dose-dependent inhibition of antifungal activity in the presence of oxidized GSH as a competing, disulphide-containing substrate (Fig. S7*C*).

redS100A7 and TPEN were identified as broad-spectrum antifungals in vitro (Fig. 1). To investigate whether both are antifungals in vivo, we developed a guinea pig tinea pedes skin model

system, allowing us to treat an experimental superficial dermatophyte infection with our agents of interest. Our results show that topical administration of either redS100A7 or TPEN prevents fungal infection in vivo (Fig. 5 *A* and *B*). In addition, in a mouse model of *Aspergillus* lung infection, in which immunocompromised mice were infected with a lethal dose of *A. fumigatus* conidia, redS100A7 or TPEN treatment prevented death from invasive fungal infection (Fig. 5 *C* and *D*). Therefore, redS100A7 and fungus cell-penetrating zinc chelators might have a therapeutical potential as novel antifungals. Lethal fungal infections are a growing threat to humans because of the increasing number of immunocompromised individuals, such as those with HIV, cancer, and transplant recipients (1–4, 38). Many antifungal agents are limited by a narrow spectrum, as well as by the development of drug resistance and toxicity, engendering an urgent need for innovative antifungal agents (1, 38).

In summary, our data represent a previously undescribed mechanism of action for an antimicrobial protein. We propose that the Cysteine-reduced form of the ubiquitous epithelial protein psoriasin (S100A7) acts as a principal human antifungal protein that induces apoptosis in fungi by penetrating the fungal cell membrane and sequestrating Zn^{2+} from an intracellular target via a newly formed thiol-based metal-binding site, which is similar to that seen with the antimicrobial peptide human defensin 5, hD5 (31). We therefore suggest that in general, fungus-cell–penetrating Zn^{2+}-chelators, like redS100A7 and TPEN, could be useful as an important new therapeutic for opportunistic, superficial, or invasive fungal infections.

Materials and Methods

Collection of human skin material was approved by the ethical committee of the Shimane University. Written informed consent was obtained from each human subject involved in this study.

Fungi were cultured in a Sabouraud liquid medium for assaying antifungal proteins. Fungal growth was photometrically measured at 595 nm. Purification of the antifungal protein from lesional psoriatic scale extracts was performed by HPLC (39, 40). Its structural identification as reduced psoriasin (redS100A7) was performed using MALDI-MS, ESI-MS, amino acid sequencing, and Western blot analyses. Psoriasin mutants were generated as SUMO-fusion proteins, which were cleaved by SUMO-protease and further purified by HPLC. Morphological studies of redS100A7- and TPEN-treated fungi were performed with TEM and SEM. For immunogold TEM, S100A7 locations in treated *T. rubrum* were identified with antibodies. Apoptosis induction was tested with the TUNEL-assay and SYTOX-green staining. In vivo activities of redS100A7 and TPEN as antifungal agents were investigated in guinea pig tinea pedis (28) and mouse *Aspergillus* lung infection models. All animal manipulations were approved by the ethical committee of Shimane University, Faculty of Medicine (approval no. 459). See *SI Materials and Methods* for full details.

ACKNOWLEDGMENTS. We thank S. Matsuki for discussions and technical help with the reactive oxygen species study; T. Yoneyama for technical help with scanning electron microscope and transmission electron microscope analyses; and Jutta Quitzau for HPLC. *A. fumigatus* ΔrodA were kindly provided by J. P. Latgé (Pasteur Institute, Paris, France). This study was supported in part by the Otsuka Toshimi scholarship foundation for postgraduate support (to K.Z.H.); a European Union, European Research Council starting grant (to J.W. and B.O.S.); a Deutsche Forschungsgemeinschaft, Reinhart Koselleck high-risk project grant (to J.M.S.); and the Cluster of Excellence "Inflammation at Interfaces" (to J.G. and S.J.).

1. Brown GD, Denning DW, Levitz SM (2012) Tackling human fungal infections. *Science* 336(6082):647.
2. Fisher MC, et al. (2012) Emerging fungal threats to animal, plant and ecosystem health. *Nature* 484(7393):186–194.
3. Brown GD, et al. (2012) Hidden killers: Human fungal infections. *Sci Transl Med* 4(165):165rv13.
4. Brakhage AA (2005) Systemic fungal infections caused by *Aspergillus* species: Epidemiology, infection process and virulence determinants. *Curr Drug Targets* 6(8): 875–886.
5. Findley K, et al.; NIH Intramural Sequencing Center Comparative Sequencing Program (2013) Topographic diversity of fungal and bacterial communities in human skin. *Nature* 498(7454):367–370.
6. Osherov N (2012) Interaction of the pathogenic mold *Aspergillus fumigatus* with lung epithelial cells. *Front Microbiol* 3:346.
7. Schroeder BO, et al. (2011) Reduction of disulphide bonds unmasks potent antimicrobial activity of human β-defensin 1. *Nature* 469(7330):419–423.
8. Henseler T, Christophers E (1995) Disease concomitance in psoriasis. *J Am Acad Dermatol* 32(6):982–986.
9. Harder J, Bartels J, Christophers E, Schröder JM (1997) A peptide antibiotic from human skin. *Nature* 387(6636):861.
10. Harder J, Schröder JM (2005) Psoriatic scales: A promising source for the isolation of human skin-derived antimicrobial proteins. *J Leukoc Biol* 77(4):476–486.
11. Gläser R, et al. (2005) Antimicrobial psoriasin (S100A7) protects human skin from *Escherichia coli* infection. *Nat Immunol* 6(1):57–64.
12. Mildner M, et al. (2010) Psoriasin (S100A7) is a major *Escherichia coli*-cidal factor of the female genital tract. *Mucosal Immunol* 3(6):602–609.
13. Meyer JE, et al. (2008) Psoriasin (S100A7) is a principal antimicrobial peptide of the human tongue. *Mucosal Immunol* 1(3):239–243.
14. Brodersen DE, Nyborg J, Kjeldgaard M (1999) Zinc-binding site of an S100 protein revealed. Two crystal structures of Ca2+-bound human psoriasin (S100A7) in the Zn2+-loaded and Zn2+-free states. *Biochemistry* 38(6):1695–1704.
15. Maret W, Li Y (2009) Coordination dynamics of zinc in proteins. *Chem Rev* 109(10): 4682–4707.
16. Michalek M, et al. (2009) The human antimicrobial protein psoriasin acts by permeabilization of bacterial membranes. *Dev Comp Immunol* 33(6):740–746.
17. Brophy MB, Hayden JA, Nolan EM (2012) Calcium ion gradients modulate the zinc affinity and antibacterial activity of human calprotectin. *J Am Chem Soc* 134(43):18089–18100.
18. Kimura E, Aoki S (2001) Chemistry of zinc(II) fluorophore sensors. *Biometals* 14(3-4): 191–204.
19. Zalewski PD, Forbes IJ, Betts WH (1993) Correlation of apoptosis with change in intracellular labile Zn(II) using zinquin [(2-methyl-8-p-toluenesulphonamido-6-quinolyloxy) acetic acid], a new specific fluorescent probe for Zn(II). *Biochem J* 296(Pt 2):403–408.
20. Radford RJ, Lippard SJ (2013) Chelators for investigating zinc metalloneurochemistry. *Curr Opin Chem Biol* 17(2):129–136.
21. Loomans HJ, Hahn BL, Li QQ, Phadnis SH, Sohnle PG (1998) Histidine-based zinc-binding sequences and the antimicrobial activity of calprotectin. *J Infect Dis* 177(3):812–814.
22. Ungpakorn R, Holdom MD, Hamilton AJ, Hay RJ (1996) Purification and partial characterization of the Cu,Zn superoxide dismutase from the dermatophyte *Trichophyton mentagrophytes* var. interdigitale. *Clin Exp Dermatol* 21(3):190–196.
23. Gamen S, et al. (2000) Doxorubicin treatment activates a Z-VAD-sensitive caspase, which causes deltapsim loss, caspase-9 activity, and apoptosis in Jurkat cells. *Exp Cell Res* 258(1):223–235.
24. Shindo Y, Witt E, Han D, Epstein W, Packer L (1994) Enzymic and non-enzymic antioxidants in epidermis and dermis of human skin. *J Invest Dermatol* 102(1):122–124.
25. Arnér ES, Holmgren A (2000) Physiological functions of thioredoxin and thioredoxin reductase. *Eur J Biochem* 267(20):6102–6109.
26. Schallreuter KU, Wood JM (1986) The role of thioredoxin reductase in the reduction of free radicals at the surface of the epidermis. *Biochem Biophys Res Commun* 136(2): 630–637.
27. Léchenne B, et al. (2007) Sulphite efflux pumps in *Aspergillus fumigatus* and dermatophytes. *Microbiology* 153(Pt 3):905–913.
28. Koga H, Nanjoh Y, Kaneda H, Yamaguchi H, Tsuboi R (2012) Short-term therapy with luliconazole, a novel topical antifungal imidazole, in guinea pig models of tinea corporis and tinea pedis. *Antimicrob Agents Chemother* 56(6):3138–3143.
29. Gaziano R, et al. (2004) Anti-*Aspergillus fumigatus* efficacy of pentraxin 3 alone and in combination with antifungals. *Antimicrob Agents Chemother* 48(11):4414–4421.
30. Lulloff SJ, Hahn BL, Sohnle PG (2004) Fungal susceptibility to zinc deprivation. *J Lab Clin Med* 144(4):208–214.
31. Zhang Y, Cougnon FBL, Wanniarachchi YA, Hayden JA, Nolan EM (2013) Reduction of human defensin 5 affords a high-affinity zinc-chelating peptide. *ACS Chem Biol* 8(9): 1907–1911.
32. Ghannoum MA, Rice LB (1999) Antifungal agents: Mode of action, mechanisms of resistance, and correlation of these mechanisms with bacterial resistance. *Clin Microbiol Rev* 12(4):501–517.
33. Nakatani T, Tawaramoto M, Opare Kennedy D, Kojima A, Matsui-Yuasa I (2000) Apoptosis induced by chelation of intracellular zinc is associated with depletion of cellular reduced glutathione level in rat hepatocytes. *Chem Biol Interact* 125(3):151–163.
34. Mendivil-Perez M, Velez-Pardo C, Jimenez-Del-Rio M (2012) TPEN induces apoptosis independently of zinc chelator activity in a model of acute lymphoblastic leukemia and ex vivo acute leukemia cells through oxidative stress and mitochondria caspase-3- and AIF-dependent pathways. *Oxid Med Cell Longev* 2012:313275.
35. Linder MB, Szilvay GR, Nakari-Setälä T, Penttilä ME (2005) Hydrophobins: The protein-amphiphiles of filamentous fungi. *FEMS Microbiol Rev* 29(5):877–896.
36. Bayry J, Aimanianda V, Guijarro JI, Sunde M, Latgé JP (2012) Hydrophobins—Unique fungal proteins. *PLoS Pathog* 8(5):e1002700.
37. Paris S, et al. (2003) Conidial hydrophobins of *Aspergillus fumigatus*. *Appl Environ Microbiol* 69(3):1581–1588.
38. Romani L (2011) Immunity to fungal infections. *Nat Rev Immunol* 11(4):275–288.
39. Schröder JM (2010) Purification of antimicrobial peptides from human skin. *Methods Mol Biol* 618:15–30.
40. Schroeder JM (2010) in *Isolation and Characterization of Human Epithelial Antimicrobial Peptides and Proteins*, eds Kabelitz D, Kaufmann SHE, *Methods in Microbiology* (Academic, Amsterdam), Vol 37, pp 115–138.
41. Espinel-Ingroff A, Chaturvedi V, Fothergill A, Rinaldi MG (2002) Optimal testing conditions for determining MICs and minimum fungicidal concentrations of new and established antifungal agents for uncommon molds: NCCLS collaborative study. *J Clin Microbiol* 40(10):3776–3781.